THE ASTROPHYSICAL JOURNAL, 455:468–479, 1995 December 20

SPECTRAL SIGNATURES OF FAST SHOCKS. II. OPTICAL DIAGNOSTIC DIAGRAMS

MICHAEL A. DOPITA[1] AND RALPH S. SUTHERLAND[2]
Received 1995 March 29; accepted 1995 June 28

ABSTRACT

In the first paper in this series, we presented a low-density grid of models of high-velocity photoionizing radiative shocks, including magnetic pressure support in the photoionization/recombination zone. Here we apply these models to the line ratios observed in narrow-line emission regions in active galaxies. From a set of line diagnostic diagrams, we find that LINER galaxies, narrow-line radio galaxies, and cooling flow emission regions can be modeled in terms of fast shocks in a relatively gas poor environment. Emission from a photoionized precursor of the shock is either weak or absent. On the other hand, the narrow-line regions associated with Seyfert 2 and 1.5 galaxies and the energetic luminous IR galaxies can be understood as fast shocks in a gas-rich environment, in which the EUV photons produced in the shock are fully, or mostly, absorbed in the shock precursor H II region. For LINER-like objects, shock velocities required range from 150 to 500 km s^{-1}, but the Seyfert spectra require shocks typically in the range 300–500 km s^{-1}. These figures are comparable to the observed line widths in both these classes of object. The magnetic parameter that characterizes these shocks is about $2 < B/n^{1/2} < 4$ μG $cm^{3/2}$, typical of the general interstellar medium. Our fast shock models are capable of explaining the long-standing "temperature problem" of active galactic nuclei, in which the electron temperatures observed are found to be systematically higher than predicted by photoionization models. For Seyfert galaxies, the preshock densities are clearly higher than the 1 cm^{-3} used in the model grid. Finally, we find evidence that nitrogen is enhanced above solar values in both Seyfert and in LINER nuclei.

Subject headings: galaxies: active — galaxies: Seyfert — shock waves

1. INTRODUCTION

All classes of active galactic nuclei (AGNs) show some evidence of "narrow-line" emission in the [O III] lines. Seyfert galaxies of classes 1 and 2 (Khachikian & Weedman 1974) both show a rich spectrum of narrow lines, as do the narrow-line radio galaxies (NLRGs). The universal characteristic of these narrow-line regions is a large [O III] λ5007/Hβ ratio ($\sim$7–20), high [O III] electron temperature (where it can be measured), the presence of He II, and strong lines of [O I], [N II], and [S II]. In addition, faint coronal lines of highly ionized species are often seen ([Ca V], [Fe X], and the like). Although the lines are termed "narrow," this is something of a misnomer, since the typical line velocity widths are in the range 200 < FWHM < 500 km s^{-1} (Costero & Osterbrock 1977), and a few objects even exceed 1000 km s^{-1} (Veilleux 1991a, b).

The other major class of narrow-line AGNs is that of the low-ionization nuclear emission-line regions, LINERs (Heckman 1980). These fall into a distinct region of excitation space when classified according to their emission-line ratios (Baldwin, Phillips, & Terlevich 1981; Veilleux & Osterbrock 1987). In particular, the [O III] λ5007/Hβ line intensity ratio is low. A defining characteristic of LINERs is that the [O III] λ5007/[O II] λ3727,9 line intensity ratio is less than unity. LINERs, or objects having LINER-like spectra, are found in the nuclei of spiral galaxies lacking nuclear starbursts (Keel 1983a, b), in as many as 50% of elliptical galaxy nuclei (Phillips et al. 1986) and in the "cooling flows" associated with first-ranked elliptical galaxies in clusters (Heckman 1981; Cowie et al. 1983; Johnstone, Fabian, & Nulsen 1987; Heckman et al. 1989). Again, typical velocity dispersions observed in all these objects are a few hundred km s^{-1}.

In the last 15 years, the hypothesis that these narrow-line regions (NLRs) of AGNs are excited by a hard power-law spectrum of UV photons has gained almost universal acceptance. In such a model, the NLRs would be excited by a fairly flat UV power law or else a truncated power law with dimensionless ionization parameter (U) typically of order 10^{-2} (Koski 1978; Stasinska 1984; Veilleux & Osterbrock 1987; Osterbrock, Tran, & Veilleux 1992; Baum, Heckman, & van Breugel 1992). If LINERs are photoionized, then again, the ionizing spectrum must be fairly flat, but in these objects the ionization parameter is low, $U \sim 10^{-4}$ (Ferland & Netzer 1983; Binette 1985; Ho, Filippenko, & Sargent 1993). The source of these photons is assumed to be the nucleus, but the exact means whereby the nonthermal UV spectrum is generated remains obscure. Generally what is done is either to join the observed soft X-ray to the region just above the Lyman limit or else to extrapolate the FUV slope with some sort of cutoff to match the soft X-ray region of the spectrum. Neither of these procedures properly addresses the physical processes producing the emission, and there remains a serious shortfall in the estimated number of ionizing photons based on an extrapolation of the observed UV spectrum (Binette, Parker, & Fosbury 1995). More recently, Barvainis (1993) has suggested that an optically thin thermal brehmsstrahlung spectrum might supply the required EUV photons. This model supplies a physical mechanism but leaves the physical structure of the EUV source uncertain.

Despite a deal of success in describing the general character of the emission-line spectrum, the weaknesses of photoionization models are that a number of parameters are relatively unconstrained. In the presence of clumping and density variation, it is difficult to understand the relatively small range of ionization parameter that is observed within each class of

[1] Mount Stromlo and Siding Spring Observatories, Institute of Advanced Studies, The Australian National University, Private Bag, Weston Creek P.O., ACT 2611, Australia.
[2] Joint Institute for Laboratory Astrophysics, University of Colorado, Campus Box 440, Boulder, CO 80309.

object, or over a very large radial scale range within individual object. Furthermore, clear correlations are seen between observed spectral characteristics and dynamics in various classes of object (Costero & Osterbrock 1977; Baum et al. 1992; Crawford & Fabian 1992). These have no place in pure photoionization models.

A promising model for all these classes of object is based on the input of mechanical energy, rather than on photoionization from a central source. The source of the mechanical energy may be either from turbulent motions of clouds in the potential of the galaxy or through direct energy disposition from an outflowing jet or bubble of relativistic electrons. This idea is by no means new. Osterbrock (1971) argued for shocks as a means to set up the multiphase structure of AGNs, and Daltabuit & Cox (1972) pointed out how such high-velocity shocks in a turbulent medium could of themselves provide an ample supply of ionizing photons.

The basic physics of this idea is quite simple. A fast, radiative shock in interstellar space is a powerful source of ionizing photons. These photons are produced in the hot, postshock plasma as it cools and can diffuse both upstream and downstream. Photons diffusing upstream encounter the preshock gas and may produce an extensive precursor H II region, while those finding their way downstream will profoundly influence the ionization and temperature structure of the recombination region of shock. Since much of the available enthalpy is radiated in this photon field, the photoionization effects produced by this diffuse UV field may dominate the optical emission produced by the cooling region of the shock itself. An early attempt to investigate the effects of radiative transfer in thermally unstable cooling flows or fast radiative shocks was given by Binette, Dopita, & Tuohy (1985). Hybrid models for fast shocks with an externally imposed photoionizing field have been extensively discussed in a series of papers (Contini & Aldrovandi 1983, 1986; Aldrovandi & Contini 1984, 1985; Contini & Viegas-Aldrovandi 1987; Viegas-Aldrovandi & Contini (1989a, b), and these have been extensively applied to the interpretation of narrow emission-line regions of active galaxies.

An accurate treatment of the internal radiative transfer in fast shocks was accomplished in the code MAPPINGS II (Sutherland & Dopita 1993). Sutherland, Bicknell, & Dopita (1993) applied this to the interpretation of the optical spectra of the filaments associated with the radio jet of Cen A. The successful application of this model to one particular case of optical emission associated with a galactic jet raises the promise that such models may be generally applicable to narrow emission-line regions in active galaxies, and this is the motivation of the current series of papers. In the first paper of this series (Dopita & Sutherland 1996, hereafter Paper I), we presented an extensive grid of magnetohydrodynamic shocks in the low-density limit. Here our object is to apply these results to the global interpretation of AGN, LINER, and cooling flow spectra.

2. THE MODEL GRID

2.1. *Parameter Space Covered*

In the grid of Paper I we presented results for a solar abundance set of low-density [$N(\mathrm{H}) = 1\ \mathrm{cm}^{-3}$] radiative steady-flow shocks and their photoionized precursors covering the range of shock velocities $150 \leq V_s \leq 500\ \mathrm{km\ s}^{-1}$. In that paper, we were able to show that the "seed" transverse magnetic field in the preshock gas provides enough pressure in the cooled zones of the shock to provide magnetic support, limiting the compression in the shock, and profoundly influencing the output spectrum. Assuming that the magnetic field, B, is frozen into the flow, the maximum compression factor produced by the shock is

$$\frac{n_f}{n} = \frac{(8\pi\mu m_{\mathrm{H}})^{1/2} V_s}{(B/n^{1/2})},$$

Where μ is the mean molecular weight and m_{H} is the mass of a hydrogen atom. This illustrates the importance of the magnetic parameter $B/n^{1/2}$. Likely values of this ratio can be estimated on the assumption that the magnetic field in the preshock ISM becomes saturated when the magnetic rigidity is high enough to damp out the turbulence. This condition is met when the Alfvén velocity is of the same order of magnitude as the thermal sound speed, and this is equivalent to equipartition between the magnetic and thermal pressures. For the warm interstellar medium in the solar neighborhood, having a sound speed $\sim 8\ \mathrm{km\ s}^{-1}$, the total magnetic field (including both transverse and longitudinal components) is therefore typically of order

$$\left(\frac{B}{\mu\mathrm{G}}\right) \sim 3\left(\frac{n}{\mathrm{cm}^{-3}}\right)^{1/2}.$$

The shock models are computed in the range $0 < B/n^{1/2} < 4\ \mu\mathrm{G\ cm}^{3/2}$.

In photoionization models, the parameters that have the largest influence on the emergent spectrum are, apart from chemical abundances, the spectral index or hardness of the radiation field and the ionization parameter, U. In photoionizing shock models the corresponding parameters are shock velocity (which controls the flatness of the UV field) and the magnetic parameter, which controls the effective ionization parameter in the optically emitting photoionization-recombination region of the shock.

2.1. *Scaling Relations*

In Paper I, we derived a number of scaling relations which are useful in the interpretation of observational results, which we collect here for convenience of the reader. First, for the shock, the total radiative flux, and the flux in the Balmer lines scales simply as the shock velocity and the density:

$$L_T = 2.28 \times 10^{-3}\left(\frac{V_s}{100\ \mathrm{km\ s}^{-1}}\right)^{3.0}\left(\frac{n}{\mathrm{cm}^{-3}}\right)\ \mathrm{ergs\ cm}^{-2}\ \mathrm{s}^{-1}, \tag{2.1}$$

$$L_{\mathrm{H}\beta} = 7.44 \times 10^{-6}\left(\frac{V_s}{100\ \mathrm{km\ s}^{-1}}\right)^{2.41}\left(\frac{n}{\mathrm{cm}^{-3}}\right)\ \mathrm{ergs\ cm}^{-2}\ \mathrm{s}^{-1}. \tag{2.2}$$

The first relation is simply the expression that all the flux of mechanical energy through the shock is radiated, while the second is related to the number of recombinations that occur in the plasma column behind the shock. At low velocities, it is dominated simply by the cooling, but as the shock velocity increases, the fraction of recombinations resulting from prior photoionizations by EUV photons increases. The net efficiency of the shock in producing Hβ photons decreases slowly with shock velocity.

The strength of the UV field escaping into the gas ahead of the shock is a strong function of shock velocity. In terms of luminosity, the steady-flow radiation field (over 4π sr) scales as

$$L_{\rm UV} = 8.87 \times 10^{-6}\left(\frac{V_s}{100\ {\rm km\ s^{-1}}}\right)^{3.04}\left(\frac{n}{\rm cm^{-3}}\right)\ {\rm ergs\ cm^{-2}\ s^{-1}}\ . \tag{2.3}$$

The precursor H II region is characterized by a high ionization with the dimensionless ionization parameter U in the range $1.5 \times 10^{-3} \leq U \leq 8 \times 10^{-3}$. As a consequence, species such as [O III] are particularly strong. The Hβ luminosity of the precursor H II region scales in much the same way as the shock itself:

$$L_{\rm H\beta} = 9.85 \times 10^{-6}\left(\frac{V_s}{100\ {\rm km\ s^{-1}}}\right)^{2.28}\left(\frac{n}{\rm cm^{-3}}\right)\ {\rm ergs\ cm^{-2}\ s^{-1}}\ . \tag{2.4}$$

Thus for velocities in excess of 200 km s^{-1} (see eq. [2.2]), the precursor is typically about 10%–20% brighter than the shock in Hβ.

3. A REFERENCE MODEL SEQUENCE

In the following section, we examine a number of specific line ratio diagnostics. However, in order to show the systematics of the shock spectra in the optical, both with and without precursor regions, we have collected into Table 1 the optical spectra produced by models at 150, 200, 300, and 500 km s^{-1} for a magnetic parameter of $B/n^{1/2} = 2\ \mu$G cm$^{3/2}$. Note that the effect of adding a precursor is principally to increase the relative intensities of [O III] and [Ne III]. However, at high shock velocity, lines such as [Ar IV],]Ar V], and [Ne V] are also enhanced in the high-ionization parameter precursor region.

Certainly the shocks without precursors (and even the ones with precursors that have shock velocities less than about 250 km s^{-1}) would be classified as LINER-like spectra. On the other hand, the shocks with precursors produce a much more Seyfert-like spectrum, as was first demonstrated by Sutherland et al. (1993).

Some differences between the model shock spectra and those of both LINERs and Seyfert galaxies are apparent. In particular, note that the un-ionized species [C I], [N I], and [O I] are predicted, in general, to have stronger lines than are generally observed. If the basic thesis that the narrow-line regions of LINERs and Seyfert galaxies are shock excited is correct, this suggests that the temperature predicted in the shock models is too high in the regions in which these species dominate, i.e., far into the recombination region of the shock. One possibility is that molecular hydrogen and other molecular species are being formed in this warm region. These provide extra coolants and effectively supress the optical forbidden lines of the neutral species. We return to this point below.

TABLE 1

SAMPLE OPTICAL SPECTRA OF RADIATIVE SHOCKS AS A FUNCTION OF VELOCITY

Line:		Shock Velocity (km.s^{-1}):			(s = *Shock only*,	sp = *Shock + Precursor*)		
λ	Ion	150s	200s	200sp	300s	300sp	500s	500sp
3426	[Ne V]	5.4	29.5	13.1	15.4	8.1	6.9	39.2
3727+	[O II]	617.4	560.6	314.2	834.3	432.8	1230	659.6
3869	[Ne III]	30.6	30.8	19.2	51.0	50.7	98.8	146.4
3934	Ca II	1.4	4.4	2.2	14.3	6.8	27.2	13.6
3963	Ca II	0.8	2.3	1.2	7.5	3.6	14.1	7.1
4069+	[S II]	4.2	5.7	2.8	10.4	5.0	13.6	7.3
4100	Hδ	24.9	25.3	25.3	25.5	25.6	25.4	25.7
4340	Hγ	45.5	45.9	46.0	46.2	46.3	46.0	46.5
4363	[O III]	18.0	12.2	5.5	7.2	4.6	4.5	15.7
4686	He II	4.6	5.1	5.2	12.4	11.9	20.9	28.4
4711+	[Ar IV]	0.9	0.8	0.5	0.5	4.2	0.3	25.3
4861	Hβ	100.0	100.0	100.0	100.0	100.0	100.0	100.0
4959	[O III]	62.2	45.2	55.0	34.5	159.8	54.7	437.5
5007	[O III]	179.1	130.1	158.2	99.7	460.4	157.4	1260
5199+	[N I]	8.8	12.5	5.8	40.6	19.4	58.3	39.4
5577	[O I]	0.7	1.0	0.5	4.3	2.1	9.8	6.3
5755	[N II]	2.8	2.5	1.2	3.6	1.8	6.2	3.3
5876	He I	6.7	15.0	14.5	19.6	15.2	18.7	13.8
6300	[O I]	38.2	70.3	33.4	249.6	119.6	394.2	195.5
6312	[S III]	1.1	1.3	0.9	1.8	1.3	3.3	2.3
6363	[O I]	12.7	23.4	11.1	83.2	39.9	131.4	65.1
6548	[N II]	43.4	71.7	41.7	118.2	59.9	158.2	83.3
6563	Hα	309.2	300.5	298.6	294.8	292.9	299.3	291.4
6584	[N II]	127.7	211.1	123.0	348.0	176.5	465.9	245.7
6678	He I	1.9	4.2	4.1	5.6	4.4	5.2	3.9
6717	[S II]	80.1	109.6	54.8	173.0	82.7	175.6	95.1
6731	[S II]	57.2	77.3	38.5	127.0	60.5	134.0	71.9
7007	[Ar V]	0.2	0.3	0.1	0.1	0.2	0.1	3.1
7136	[Ar III]	3.5	9.6	10.5	18.4	17.8	28.7	20.3
7325+	[O II]	26.7	19.8	9.2	16.1	8.0	22.8	12.2
9069	[S III]	11.5	27.8	32.8	54.0	42.3	87.4	54.8
9532	[S III]	28.1	67.6	79.9	131.4	102.9	212.9	133.5
9851	[C I]	84.8	37.4	16.8	63.5	28.9	59.8	29.6

4. DIAGNOSTIC PLOTS

The utility of plotting pairs of emission-line ratios as a tool for plasma diagnostics and classification of emission-line objects has been amply demonstrated over the years. Baldwin et al. (1981) were the first to demonstrate how this procedure could be used to separate the various classes of active galactic nuclei. However, such diagrams had been used for many years before this in the separation of H II regions from shock-excited plasmas or for abundance diagnostics of emission nebulae (e.g., Sabbadin, Minello, & Bianchini 1977; D'Odorico 1978; Dopita 1977, 1978). Veilleux & Osterbrock (1987) emphasized the importance of choosing line ratios that are as close together in wavelength as possible to avoid errors due to reddening corrections or errors in instrumental sensitivity calibrations. A number of authors have used diagnostic line ratio diagrams using only emission lines in the red region of the spectrum, where reddening effects and measurement problems are minimized. Among these we note the use of the [S II] line ratio and the [S III] lines in the separation of shock and photoionization heating mechanisms in active galaxies by Diaz, Pagel, & Terlevich (1985a), Diaz, Pagel, & Wilson (1985b), and Kirhakos & Phillips (1989). Different diagrams have been used by Baum et al. (1992) in the interpretation of emission-line nebulae in radio galaxies and by Osterbrock et al. (1992) in the separation of Seyfert 2 nuclei, LINERs, starburst galaxies, and narrow emission-line galaxies of uncertain classification.

Here we will compare our models with observations of active galaxies on diagnostic plots taken from Baldwin et al. (1981), Veilleux & Osterbrock (1987), Osterbrock et al. (1992), and Baum et al. (1992).

Before this is done, it should be noted that the comparison grid is for a fixed, solar abundance set, and for the low-density limit. Real objects show large density differences one from another (Koski 1978), and the chemical abundances of the host galaxies are certain to show at least an order of 2 variation. As a consequence, a "good" fit should be regarded as better than 0.3 dex in the important line ratios. The scales of the diagnostic plots are chosen only so as to fit the grid and the observed points and are more restrictive than comparisons that include starburst galaxies and H II regions as well.

4.1. *Data Sources*

In the following plots, spectrophotometric data for Seyfert 2 and 1.5 galaxies have been drawn from Veilleux & Osterbrock (1987) and Osterbrock et al. (1992), supplemented by data from Costero & Osterbrock (1977), Shuder & Osterbrock (1981), Koski (1978), Morris & Ward (1988), Tadhunter, Robinson, & Morganti (1989) and Storchi-Bergmann, Kinney, & Challis (1995). For LINERs we use data from Veilleux & Osterbrock (1987) and Osterbrock et al. (1992), supplemented by data from Koski (1978), Keel (1983a, b), Ho et al. (1993), and Storchi-Bergmann, Kinney, & Challis (1995). The data on radio galaxies come from Baum et al. (1992), and the spectrophotometry of cooling flows is from Crawford & Fabian (1992).

4.2. *Results*

[O III] λ5007/Hβ *vs.* [O II] λ3727,9/[O III] λ5007 (*Fig.* 1).—This is one of the Baldwin, Phillips, & Terlevich plots which is particularly useful in separating H II regions and planetary nebulae from AGNs. Active galaxies are characterized by stronger [O III] lines for a given oxygen ionization degree. Our results for shocks and for shocks with their precursors are plotted in Figure 1. A good separation of the two types of shock is achieved on this diagram. The Seyfert galaxies are found in the region of the shock + precursor, and shock velocities typically in the range 300–500 km s^{-1}. The LINER galaxies are found in the left-hand side of the region of the shock-only models. However, it is not possible to determine from this diagram what characteristic velocity is required. An increase in the electron density would lead to a weakening of the [O II] line. This would shift points to the left on this diagram and also tend to increase the scatter of the observational points. Since varying the magnetic parameter also produces a displacement along the x-axis, nothing useful can be inferred about the likely value of the magnetic parameter from this diagram.

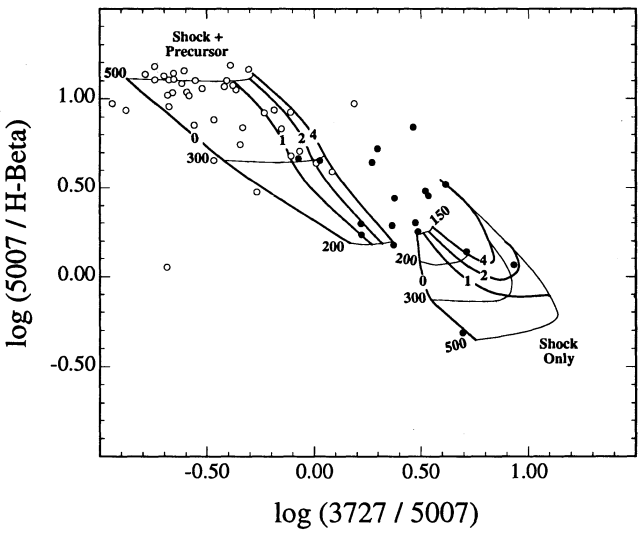

FIG. 1.—The [O III] λ5007/Hβ ratio vs. [O II] λ3727,9/[O III] λ5007. Theoretical grids of shock models are compared with observations for Seyfert galaxies (*open circles*) and of LINERs (*filled circles*) from the literature. The grid marked "shock only" is the contribution from the radiative shock only, and the grid marked "shock + precursor" includes the contribution of the H II region ahead of the shock front photoionized by the upstream EUV photons. The grids are labeled in terms of their shock velocity (150–500 km s^{-1}) and their magnetic parameter $B/n^{1/2}$ (0–4 μG cm$^{3/2}$). Note that the significance of this and succeeding plots are discussed fully in the text.

[O III] λ5007/Hβ *vs.* [S II] $\lambda\lambda$(6717+6731)/Hα (*Fig.* 2*a*).—This is one of the Veilleux & Osterbrock (1987) diagnostic plots, along with Figures 2*b* and 2*c*. Again a clear separation of the shock + precursor and shock-only regions is achieved. These clearly correspond to the Seyfert and LINER regions, respectively, with shock velocities are in the range 150–500 km s^{-1} for the LINERs and 250–500 km s^{-1} for the Seyfert galaxies. There is clear evidence for weakening of the [S II] through collisional deexcitation, giving the observed spray of Seyfert points to the left of this diagram. Densities observed for the Seyfert galaxies from the ratio of the sulfur lines lie up to log $n_e \sim 4.2$ in the Koski (1978) sample. The interpretation of what this density means is a little complex in radiative shocks with precursors. As the density of the material passing through the shock increases, the density indicated by the [S II] ratio also increases, to be sure. However, the amount of compression depends critically upon the magnetic parameter, and shocks with $B/n^{1/2} = 2$ μG cm$^{3/2}$ remain near the low-density limit up to $n \sim 10$ cm^{-3}. Consider the case of 500 km s^{-1}. At preshock densities of 1, 10, and 100 cm^{-3}, the [S II] ratios $\lambda\lambda$(6731/6717) given by the shock + precursor structure are 0.7559, 0.8569,

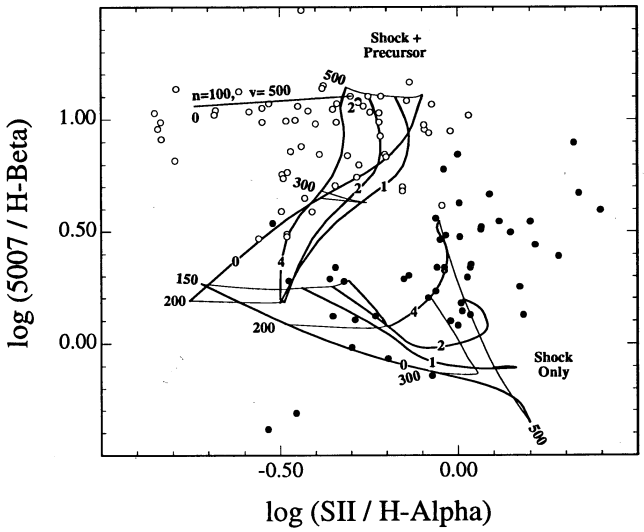

FIG. 2a

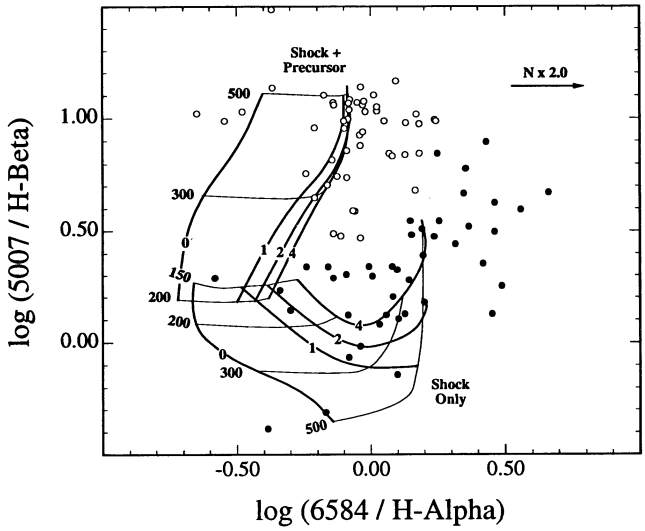

FIG. 2b

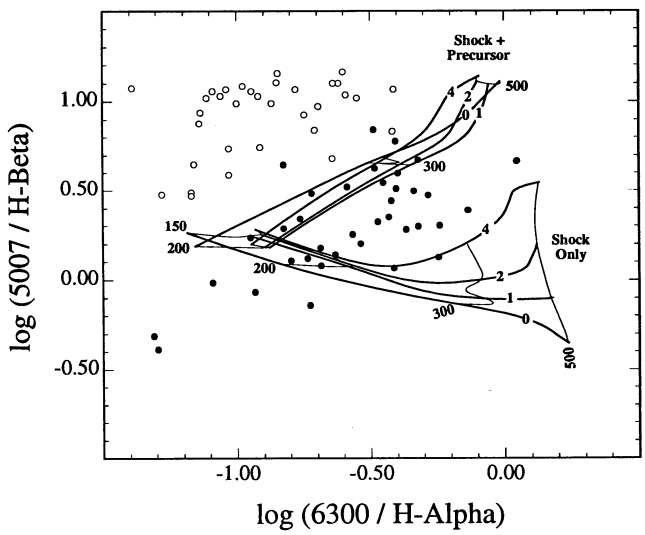

FIG. 2c

FIG. 2.—(*a*) As Fig. 1, but for the ratios [O III] λ5007/Hβ vs. [S II] λ6717,31/Hα. The effect of collisional deexcitation of [S II] is indicated for two models having a shock velocity of 500 km s^{-1}, a preshock hydrogen density of 100 cm^{-3}, and magnetic parameter, $B/n^{1/2} = 0$ and 2 μG $cm^{3/2}$, respectively. (*b*) As Fig. 1, but for the ratios [O III] λ5007/Hβ vs. [N II] λ6584/Hα. The effect of a factor of 2 increase in the N/O ratio is shown by the arrow. For both grids, this produces negligible shift in the vertical axis. (*c*) As Fig. 1, but for the ratios [O III] λ5007/Hβ vs. [O I] λ6300/Hα.

and 1.527, respectively. However, for $B/n^{1/2} = 0$ μG $cm^{3/2}$ the [S II] ratio is already 1.288 with a preshock density of 1 cm^{-3}. For still higher postshock densities, the collisional deexcitation can become so severe as to leave only the precursor contribution to the [S II] lines. At highest densities, even this will be collisionally deexcited. As a consequence, with increasing preshock density we would expect a continuously decreasing relative intensity of the [S II] lines to be accompanied by first an increase in the apparent [S II] ratio, then a decrease, and finally another increase to the high-density limit. These effects will be fully investigated in a future paper. However, to demonstrate the nature of this effect, we have plotted the positions of two 500 km s^{-1}, $n \sim 100$ cm^{-3} models having magnetic parameters $B/n^{1/2} = 0$ and 2 μG $cm^{3/2}$, respectively. The collisional weakening of [S II] is very apparent.

The observational points plotted for the LINERs do not show [S II] densities greater than about log $n_e \sim 3$, so the low-density limit is a reasonable assumption for these objects. We find a number of points lying above and somewhat to the right of the grid, with up to about 0.5 dex stronger λ5007/Hβ line ratios and 0.2 dex stronger [S II]/Hα line ratios. These may be simply objects in which the Hα and Hβ lines have been underestimated due to underlying galactic stellar absorption. Phillips et al. (1986) showed how inadequate template subtraction could lead to this effect in weak-line LINERs. Another possibility is that points in this region represent transitional objects having partial preionization zones. This will be investigated, along with density effects, in the third paper of this series. Qualitatively, the effect of building up a precursor region will be first to increase the [O III]/Hβ ratio and, later, to decrease the [S II]/Hα ratio.

[O III] λ5007/Hβ *vs.* [N II] λ6584/Hα (*Fig. 2b*).—On the second of the Veilleux & Osterbrock (1987) diagnostic plots, the separation of the two classes of shock is again distinct, and these correspond closely to the regions in which LINER (no precursor) and Seyferts (shock + precursor) are observed. The systematics of the line intensity variations between objects is well described by the shock model sequence. Again, shock velocities inferred are in the range 150–500 km s^{-1} for the LINERs and 250–500 km s^{-1} for the Seyfert galaxies, and there appears to be some grounds for concluding that the magnetic parameter is fairly high ($2 < B/n^{1/2} < \sim 6$ μG $cm^{3/2}$). Note that for both classes of object there are points scattering to the right by up to 0.4 dex. This effect could be caused by a nitrogen abundance that is greater than solar. Certainly, such an increased nitrogen abundance is seen in the centers of luminous galaxies as a result of enrichment by dredge-up processes in the planetary nebular population (see review by Pagel & Edmonds 1981). To estimate this effect, we have calculated models with an enhancement of 2 in the N/O ratio. The abundance variation translates almost in a one-to-one fashion to an increase of the strength of the [N II] line, as is indicated by the arrows in this figure, and in Figures 3*a* and 3*c* (below).

[O III] λ5007/Hβ *vs.* [O I] λ6300/Hα (*Fig. 2c*).—The third of the Veilleux & Osterbrock (1987) diagnostic plots shows the poorest correspondence with observation. For both sequences, the observed points fall to the left of the theoretical lines by typically, 0.4 dex, although the slopes are reasonably well accounted for by the models. Four effects could cause this. First, the nitrogen overabundance mentioned above will directly lead to a weakening of both the [S II] and [O I] intensity ratios. This is caused by the fact that there is a certain amount of the enthalpy is available to be radiated in the low-ionization emission lines, so an increase in the strength of one line leads to a reduction in the strength of the others. However, an increase in nitrogen abundance would also lead to an increase in the [N I] line, and this is not observed.

Second, the [O I] line itself is particularly difficult to model, since the collision strength is such a sensitive function of temperature, and because the emissivity of the line is dominated, in roughly a factor of 3 to 1, by proton rather than electron excitations. The predicted intensity of this line is therefore very sensitive to the particulars of the temperature structure in the partially ionized photoionization-recombination zone of the shock. The implication is that we are overestimating the temperature in this zone.

This leads us to the third possibility, already alluded to in the previous section, that molecular species are forming in the extended warm and weakly ionized region. In MAPPINGS II, we do not treat the molecular chemistry, so we cannot check this possibility. However, if molecules such as H_2, HC^+, and CO are being formed, then collisional excitation into rotation and vibrational levels can be expected to be rapid, leading to a much cooler recombination tail to the shock structure. In this regard, the models of Shapiro, Clocchiatti, & Kang (1992) are instructive.

A fourth (and likely) possibility is that developed instabilities in the coolest parts of the shock structure have formed cloudlet and filaments. In this case the effect of the X-ray ionization that is both maintaining the high electron temperatures and driving the [O I] line intensity becomes much less important. These instabilities may be either secondary shocks produced by thermal instabilities, magnetic instabilities, or Kelvin-Helmholtz or Rayleigh-Taylor instabilities.

[N II] λ6584/Hα *vs.* [S II] $\lambda\lambda$(6717+6731)/Hα (*Fig. 3*).—This ratio is closely related to the ratios used by Baum et al. (1992) for radio galaxies. On Figure 3*a*, we plot points for radio galaxies derived from Heckman et al. (1992) as crosses, to distinguish them from the LINER galaxies (*filled circles*). From this it appears that these two classes of object are characterized by identical ratios, suggesting that a common ionization source is a play. The theoretical line ratios for the shock only sequence are overlaid. The high magnetic parameter models $2 < B/n^{1/2} < 4$ μG cm$^{3/2}$ with varying shock velocity reproduce the observed slope with a high precision, although it is clear from the plot that some objects show stronger [N II] lines than are modeled. This is consistent with our conclusion above that some LINERs have higher than solar nitrogen abundances. A factor of about 2 increase in nitrogen abundance would allow the theory to encompass virtually all points on this diagram, as can be seen from the vector shown on Figure 3*a*. Shock models do a much better job in reproducing both the observed intensity of the lines and the slope of the correlation than do photoionization models, which would require a flattening of the photoionizing spectrum at a constant ionization parameter to reproduce the observed trend (see Baum et al. 1992; Ho et al. 1993). It is difficult to imagine a physical cause for such a variation.

Interestingly enough, a number of other classes of object also lie on the correlation defined by LINERs and NLRGs. In Figure 3*b*, we plot these classes, the luminous IR (LIR) galaxies with velocity greater than 250 km s^{-1} taken from Armus, Heckman, & Miley (1989) and the cooling flows observed by Crawford & Fabian (1992) on the same axes as Figure 3*a*. Different cooling flows are characterized by a relatively small dispersion in shock velocity, if this is indeed the excitation mechanism. However, the range of line ratios and the absolute values defined by the cooling flows and LIR galaxies are essentially the same as for LINERs and for radio galaxies, which strongly suggests that a common excitation mechanism is at play. The cooling flows are particularly interesting for testing the shock excitation hypothesis, since the spatial resolution that can be achieved in these objects is sufficient to test for correlations between line ratios and velocity dispersion. A number of the Crawford & Fabian (1992) cooling flows show such a correlation, and in the correct sense, viz., an increase in the [N II] or [S II] line strengths with respect to Hα is correlated with an increase in the velocity dispersion. Such an effect has no place in photoionization models.

Similar correlations are observed both within and between LIR galaxies (Veilleux et al. 1995), which suggest that shocks also have an important role to play in these objects as well. This point is discussed in more detail in § 5 (below).

In Figure 3*c* we plot the shock + precursor model grid along with the Seyfert observational points on the same diagram. Note that only a weak separation between the two grids is achieved on this plot, but that the observed points fit quite well provided that, again, a $\sim$2 times overabundance of nitrogen is assumed.

[O II] $\lambda\lambda$(7318+7324)/Hα *vs.* [S II] $\lambda\lambda$(6717+6731)/Hα (*Fig. 4*).—This is one of the diagnostic plots of Osterbrock et al. (1992). Although the separation between the two theoretical grids is not very large, the theoretical sequences fall much closer to the region of the observed points than do the photoionization models used in that paper (Stasinska 1984), and also the small variation of the [O II] ratio is explained by the shock model. The relatively strong [O II] in these models is a consequence of the contributions of both the cooling zone and the warmer parts of the photoionization-recombination zone of the shock. The fact that the Seyfert points lie above the shock + precursor sequence is another consequence of the effects of collisional deexcitation in these higher density objects, which moves points both toward stronger [O II] λ7320 and weaker [S II] lines.

[S III] $\lambda\lambda$(9069+9531/Hα *vs.* [S II] $\lambda\lambda$(6717+6731)/Hα (*Fig. 5*).—This is another line ratio used by Osterbrock et al. (1992) and has the advantage of comparing the two observable ionization stages of sulfur. In Figure 5*a* we plot the shock-only grid along with the LINER points, and in Figure 5*b*, we give the Seyfert observations along with the shock + precursor grid. The agreement of the shock only grid with the LINER objects is excellent. It is important to note that a criticism of the shock models has been that they are unable to reproduce the observed strength of the [S III] lines in the sense that they are predicted to be too weak. This is clearly not the case, once the autoionization effects are properly taken into account. On the other hand, photoionization models overestimate [S III], and as Ho et al. (1992) point out, "no combination of U, n, or α appears capable of rectifying the discrepancy." The

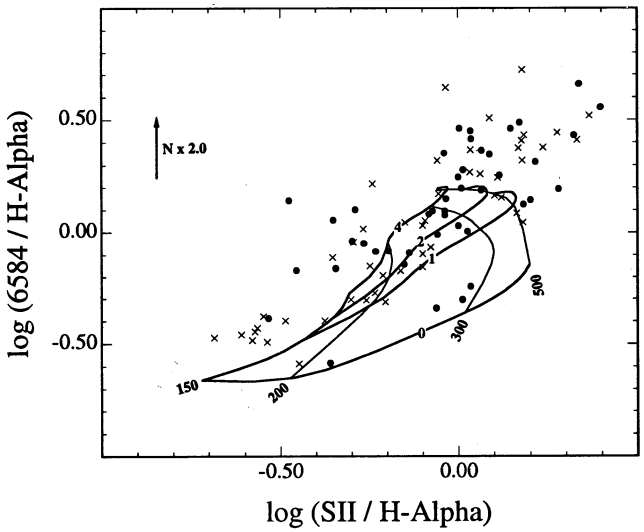

FIG. 3a

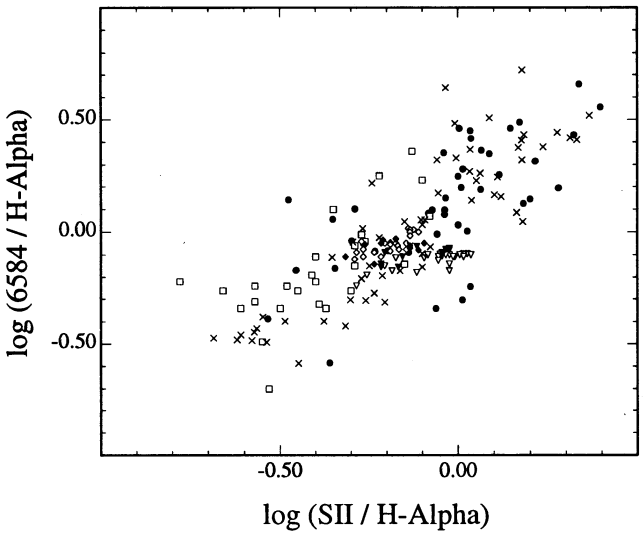

FIG. 3b

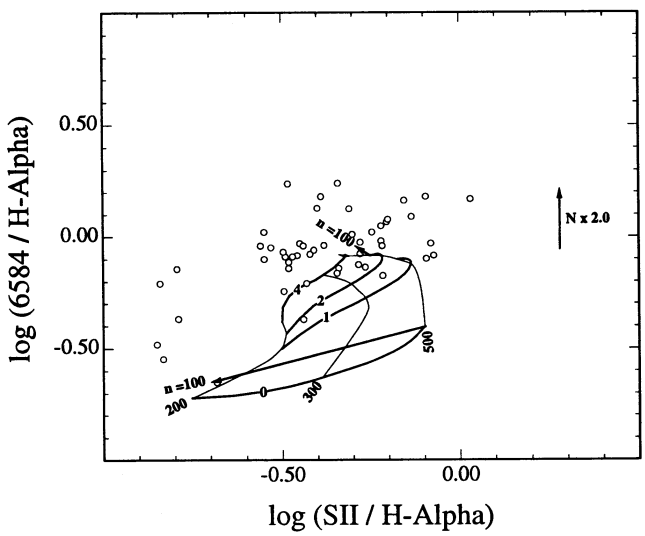

FIG. 3c

FIG. 3.—The ratios [N II] λ6584/Hα vs. [S II] λ6717,31/Hα. Here the "shock-only" grid is compared with LINER (*filled circles*) and the radio galaxies of Baum et al. (1992) (*crosses*). The effect of a factor of 2 increase in the N/O ratio is shown by the arrow. (*b*) As (*a*), but here we have plotted LINERs (*filled circles*) and the radio galaxies of Baum et al. (1992) (*crosses*), the luminous IR galaxies having observed velocity dispersions greater than 250 km s^{-1} from Armus, Heckman, & Miley (1989) (*open squares*) and individual cooling flows observed by Crawford & Fabian (1992) (*all other symbols*). Normal H II regions would be found below and to the left of all points on this diagram. This diagram emphasizes the possibility of a common source of excitation in all these disparate classes of objects. (*c*) As (*a*), but comparing the "shock + precursor" grid with observations of Seyfert galaxies (*open circles*). The effect of a factor of 2 increase in the N/O ratio is indicated, and the effect of high density is indicated by arrows for shock velocity 500 km s^{-1}, a preshock hydrogen density of 100 cm^{-3}, and magnetic parameter, $B/n^{1/2} = 0$ and 2 μG $cm^{3/2}$, respectively.

shock + precursor sequence also gives a fine fit to observations of Seyfert galaxies, especially when it is remembered that sulfur is collisionally deexcited (compare, for example, with Fig. 2*a*).

He II λ4686/Hβ *vs.* [O III] λ5007/Hβ (*Fig.* 6).—In the study of planetary nebulae, it has been found that the intensities of the [O III] and He II lines depend very strongly on the excitation temperature of the central star, and as a consequence these line ratios are the principal ratios used for the definition of excitation class (see, for example, Dopita & Meatheringham 1990). Given that the lines used lie close in wavelength and are easily measured, it is curious that they have not been more frequently used in the study of AGNs. In the case of LINERs, it is difficult to find examples in which the He II line ratio has been measured, thanks to the strength of the underlying stellar continuum and the difficulties of template subtraction. Nevertheless, detections of He II are to be found in the literature. This is important in order to distinguish excitation by hot post-AGB stars (Binette 1995) from high-velocity shock excitation. In the case of Seyfert galaxies, on the contrary, most have well-measured He II line intensities. In Figure 6*a* we give the shock-only grid, and in Figure 6*b*, the shock + precursor grid compared with the observed points for Seyfert galaxies. The shock + precursor models give a good account of the obser-

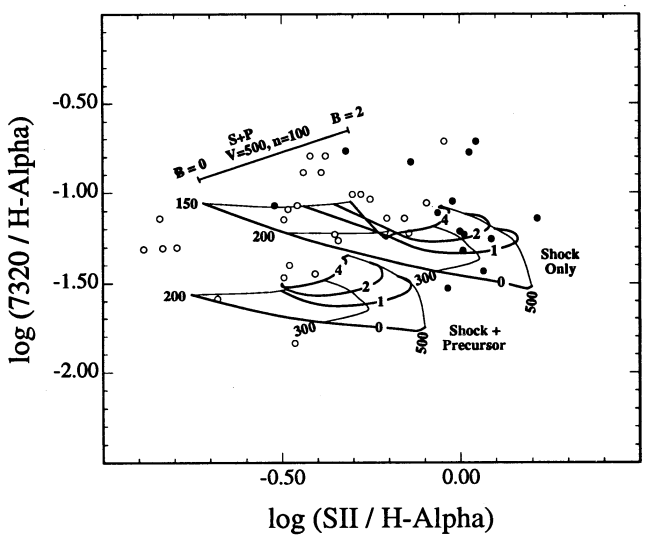

FIG. 4.—As Fig. 1, but for the ratios [O II] λ7318,24/Hα vs. [S II] λ6717,31/Hα. The effect of collisional deexcitation of and changing density structure in the recombination zone is indicated for two models having a shock velocity of 500 km s^{-1}, a preshock hydrogen density of 100 cm^{-3}, and magnetic parameter, $B/n^{1/2} = 0$ and 2 μG $cm^{3/2}$, respectively.

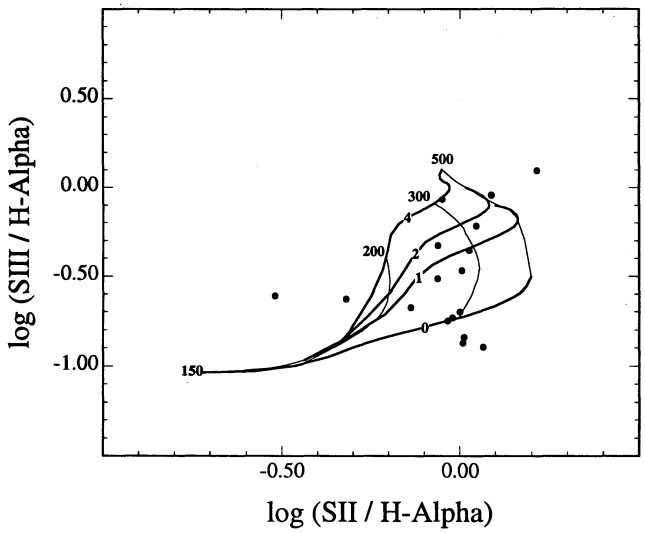

FIG. 5a

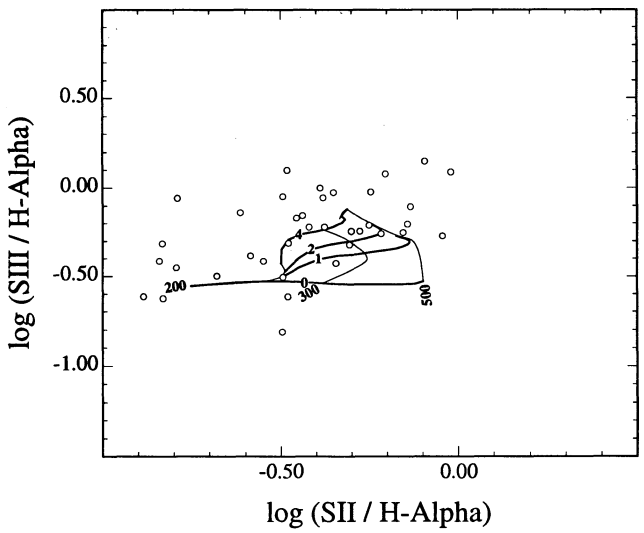

FIG. 5b

FIG. 5.—(*a*) The ratios [S III] λ9069,9531/Hα vs. [S II] λ6717,31/Hα. Here the "shock only" sequence is compared with the observations of LINERs from the literature (*filled circles*). (*b*) As Fig. 3*c*, but for the ratios [S III] λ9069,9531/Hα vs. [S II] λ6717,31/Hα. For the effects of collisional deexcitation on the [S II] lines, see Fig. 2*a*.

vations, and, since the grid is degenerate in terms of magnetic parameter, we can see that both line ratios concur that the majority of Seyfert 2 galaxies; if shock-excited, have shock velocities between 300 and 500 km s^{-1}.

[O III] λλ4363/5007 *vs.* [O III] λ5007/Hβ (*Fig.* 7).—Here we plot the temperature-sensitive [O III] line ratio against the strength of the [O III] λ5007 line. Here the data sources are drawn from those used and referred to in the discussion of the diagnostic plots above and are supplemented by data from Tadhunter et al. (1989), Fosbury et al. (1978), and the Seyfert galaxies given in Veilleux et al. (1995). For LINERs, the accuracy of the λλ 4363/5007 ratio may be suspect in cases of poor template subtraction (see Keel & Miller 1983 for a discussion of this).

A long-standing problem in AGN modeling has been the so-called temperature problem. In brief, the nature of this problem is that simple photoionization models give low temperature (~11,000 K), which disagrees strongly with observation of NLRs, for which [O III] electron temperatures are observed to range up to ~22,000 K (Tadhunter et al. 1989). This problem is not unique to Seyfert galaxies. Indeed, in the case of the prototypical LINER N1052, both Koski & Osterbrock (1976) and Fosbury et al. (1978) argued that, in order to explain the observed [O III] line ratio, shocks are essential. The distinct advantage of our self-ionizing shock model is that the shocked region itself produces significant amounts of optical radiation, particularly in respect of the [O III] λ4363 line. The emission zone of this line is strongly

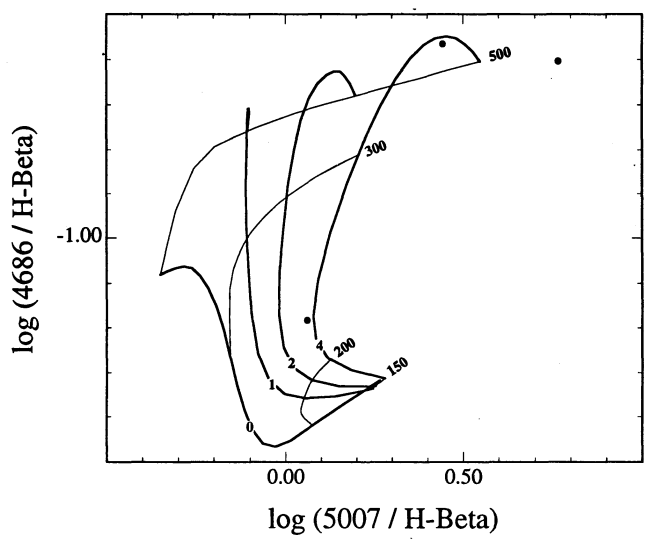

FIG. 6a

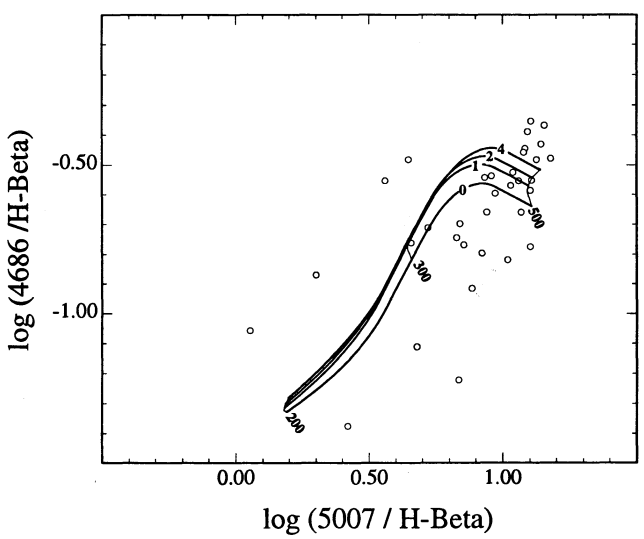

FIG. 6b

FIG. 6.—(*a*) As Fig. 5*a*, but for the ratios [O III] λ5007/Hβ vs. He II λ4686/Hβ. The He II line has not been previously used as a diagnostic tool because for LINERs this line is either faint or undetected. (*b*) As (*a*), but for shock + precursor models. As in the case of planetary nebulae, these ratios provide a very natural excitation classification tool for Seyfert galaxies.

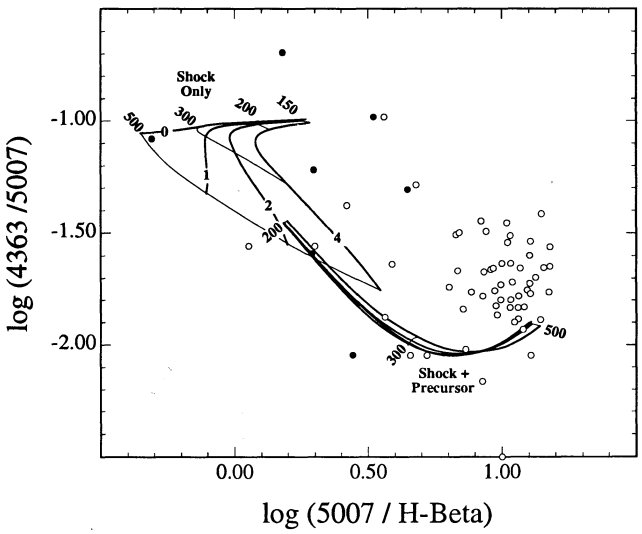

FIG. 7.—As Fig. 1, but for the ratios [O III] λ5007/Hβ vs. [O III] λ4363/λ5007.

biased to sample the hotter regions where, although the fractional abundance of the O^{++} ion may be low, the line intensity is strongly enhanced by the exponential term in the emissivity, $\exp(-\Delta E/kT)$. As a result, the electron temperature inferred for the "global" spectrum is predicted to be a good deal higher than would be given by a photoionization calculation (~17,000 K) and is in much closer agreement to what is observed. Figure 7 shows that slow shocks with precursors and bare shocks both produce stronger [O III] λ4363 lines, thanks to the enhanced contribution of the cooling zone in these models. For the sprinkling of LINERs for which we have data, and for the relatively weak line Seyferts, such a trend is evident. This is a significant result, as photoionized models predict that the electron temperature will on the contrary fall as the [O III] λ5007 line becomes weaker, since either lower values of U or steeper spectral slope of the photoionizing field, α, are required to obtain models in this region. Typical theoretical values (Tadhunter et al. 1989) of log (4363/5007) for photoionized models lie in the region −2.2 to −2.5, a factor of *50* too low!

In Figure 7, it is clear that the temperature problem is not yet fully solved, in that the theoretical curves lie, in general, below the observed points. This is not a consequence of density, since the points on this diagram are mostly derived from low-density extended emission-line regions. Optically thin precursors would display both strong [O III] lines and high values of log (4363/5007). However, this is unlikely to be the explanation for the remaining discrepancy, since these regions do not show, for the most part, any sign of optically thin precursor regions in the other diagnostic plots. The most likely cause of the difference is that most of these objects have a subsolar metallicity. This would serve to raise the temperature in both the precursor and in the cooling region. In addition, the lower cooling rate would allow a greater fraction of oxygen to recombine to O^{++} at a higher temperature, so enhancing the λ4363 line preferentially. The strong line intensities and line ratios would be little affected by, say, a factor of 2 decrease in metallicity thanks to the well-known saturation effect of principal coolants in radiative shocks (Dopita et al. 1984). We will investigate the effect of metallicity in the next paper of this series.

To achieve a definitive test of the shock models, UV observations are required. Those resonance lines which are predominantly produced in the cooling zone of the shock are predicted to be much stronger than in a photoionization model that would give a similar optical spectrum. In particular, in Paper I, we showed that the temperature-sensitive UV line ratios are expected to give an even higher temperature than the [O III] line ratio. In this respect the Hopkins Ultraviolet Telescope (Kriss et al. 1992) on NGC 1068 provide an unambiguous diagnostic. For this object the C III λλ(1907+9)/977 intensity ratio (3.51 ± 0.51) gives a temperature in excess of 27,000 K, and the N III λλ1750/991 ratio (1.47 ± 0.34) suggests temperatures in excess of 24,000 K. In addition, the absolute intensity of the C IV line is much higher than would be predicted from a photoionized model, even accounting for the flux in the broad wings, which in this object are probably derived from scattering from the hidden central object. In NGC 1068, there seems little doubt that shocks are of paramount importance in understanding the emission-line spectrum.

5. DISCUSSION

A substantial amount of line intensity information has been presented in this paper to support the hypothesis that extended emission-line regions in Seyfert 2 and 1.5 galaxies, high-luminosity radio galaxies, LINERs, cooling flows, and some luminous IR galaxies are all shock excited. If correct, this viewpoint represents a "miniunification" of AGN phenomena. However, before such a viewpoint can become generally accepted it is important to ask (1) How are these shocks driven in each class of object? and (2) What other evidence, in particular dynamical evidence, do we have for shock excitation?

We should, from the start, distinguish between two possible types of gasdynamical flow: accretion-driven and jet-driven (or wind-driven). It is almost certain that Seyfert galaxies represents jet-driven flows, one of interaction of a light, hot, or even relativistic plasma with a surrounding relatively dense and cool galactic medium. A relativistic jet might be escaping beyond the main mass concentration in a galaxy to inflate a double-lobe radio source, but it may be still entraining and shocking the cooler gas along the boundaries of the outflow. Alternatively, the density of the galactic medium may be so large as to have made the jet become completely turbulent, acting to inflate a bubble of hot gas and to drive a radiative bow shock into the general galactic medium. In the first case it provides a well-defined "ionization cone" (Pogge 1988a, b, 1989; Tadhunter & Tsvetanov 1989; Fosbury 1989) normally interpreted to be the result of beaming of UV radiation from the nucleus. This idea is an important part of the "unified models" of AGNs (Antonucci & Miller 1985; Barthel 1989). In the second case it produces a pair of more spherically symmetric bubbles of ionized gas on either side of the nucleus (e.g., M87: Sparks, Ford, & Kinney 1993; M51: Cecil 1988; 3C 277.3: van Breugel et al. 1985).

The collective effects of supernovae and mass loss from stars in starburst nuclei may also drive shocked galactic-scale bubbles. A number of these are seen in the class of LIR galaxies (Armus, Heckman, & Miley 1990). A spectactular case of such an outflow is that of NGC 3079, which displays a nuclear superbubble in very rapid expansion, and a characteristic shock-excited spectrum (Filippenko and Sargent 1992; Veilleux et al. 1994). However, even dwarf galaxies may produce such flows (Meurer, Freeman, & Dopita 1989).

The case of an entraining jet has been treated in the hydrodynamic calculations of Bicknell (1990, 1994) and applied to the case of the filaments in Cen A by Sutherland et al. (1993). In these, a mildly supersonic jet confined by a denser medium will strongly interact with the surrounding medium through the operation of the Kelvin-Helmoltz instability at the boundary. This generates slow shocks in the surrounding medium, and turbulent vortices pull off dense clouds of gas embedded in a lower density phase that is partially entrained in the jet. The turbulent collisions of clouds generate fast shocks, and slower shocks are driven into them.

In both bubble-driven flows or in entraining jet-driven flows, we would expect to find a number of global and local correlations peculiar to the shock-excited model. Because the hot plasma is confined by the cooler, we would expect to find the optical emission surrounding any radio lobes in regions in which the wall density is sufficient to allow the shocks to become radiative. Because the brightness of the radiative shock and its precursor scales as the rate of dissipation of mechanical energy through it, we would expect to find a strong correlation between local velocity dispersion and local surface brightness. Both the bubble-driven and the jet-driven flow will be distinguished by a global outflow velocity in the lobes, superposed on the local rotation curve, whereas the photoionized case will show only rotation. In the shock-excited case the excitation of the narrow-line region will be a strong function of the local velocity dispersion and/or outflow velocity, highly shocked regions having higher excitation, and showing stronger forbidden lines with respect to the Balmer lines. Because we would expect the shocks to be driven by the pressure in the relativistic plasma, we would expect to find similar pressures in the relativistic and NLR gas. Radiative shocks in general are efficient producers of forbidden lines. Thus, to the extent that the radio emission is a measure of the gas pressure in the lobes, we would expect to see a correlation of the flux in these lines with the radio luminosity.

In fact, all of the properties of entraining jet-driven flows listed above are encountered in various well-observed NLRs. However, what is not yet so clear is that these properties are universal to all NLRs. The papers that could be referenced here are legion, so the sample we now quote should be taken as simply giving examples of each phenomenon. Close correlations between the forbidden-line regions and the radio continuum regions are found in the sample of nearby Seyfert galaxies studied in the extensive survey by Tsvetanov, Fosbury, & Tadhunter (1995). In particular, there is often an excellent alignment with inner radio jets (Unger et al. 1987; Wilson & Tsvetanov 1994). Higher redshift and more luminous sources likewise show strong alignments between the NLR and the radio (McCarthy et al. 1987; Baum et al. 1988; Meisenheimer, Hippelein, & Neeser 1994). Evidence of balance between the thermal pressure in the NLR gas and the relativistic and magnetic pressure in the lobes was found by De Bruyn & Wilson (1978) and Unger et al. 1987). Correlations of line flux with radio luminosity were found by Baum & Heckman (1989; [N II] + Hα), Forbes & Ward (1993; [Fe II]), and Morganti et al. (1994; [O III]). A dynamical correlation between the [O III] line width and the radio luminosity was found for high-luminosity sources by Wilson & Willis (1980) and Whittle (1992, 1994). Evidence for global outflow and for line splitting and broadening of several hundred km s^{-1} has been found in many objects. To give a few particular examples, 3C 120 (Meurs et al. 1989), NGC 1068 (Antonucci & Miller 1985; Cecil & Bland 1989), NGC 3516 (Mulchaey et al. 1992; Veilleux, Tully, & Bland-Hawthorne 1993), N2992 (Tsvetanov, Allen, & Dopita 1995), and the LIR galaxy NGC 3079 (Veilleux et al. 1994). Examples of "twisted" jets are even seen to exist, along with strong evidence for shock excitation (Cecil, Wilson, & Tully 1992; Cecil, Morse, & Veilleux 1995). A relationship between the surface brightness and level of excitation of the NLER was discussed by Fosbury (1989) and Prieto, di Serego Alighieri, & Fosbury (1989), and Koekemoer et al. (1994) showed that a flux–velocity dispersion relationship exists for the NLERs of luminous radio galaxies. The LIR galaxy NGC 3079 shows double correlations between the surface brightness, the level of excitation measured by the [N II]/Hα ratio and the local velocity dispersion. An example of a line width–excitation correlation between the high-velocity dispersion LIR galaxies observed by Armus et al. (1989) is shown in Figure 8, and other examples of such correlations are given for LIR galaxies in Veilleux et al. (1995), Figure 41.

In accretion-driven flows, the shock is either the result of the collision of cool clouds which have dropped out of a cooling flow into the potential of the galaxy or have been accreted from a companion galaxy in a merger. Shocks may also occur in the outer accretion disk about the central object either through the dissipation of turbulence, dynamical instabilities, or spiral shocks. In the case of cooling flows, clear evidence for shock excitation was found by Crawford & Fabian (1992). Apart from the correlation between velocity dispersion and [N II]/Hα already alluded to above, they found a strong relationship between the local velocity dispersion and the local surface brightness of the emission. This can be fitted closely to the theoretical slope of 2.4, which follows that expected from equation (2.1), applied to Hα. Of course, a great deal of scatter is expected in such a relation, since the surface brightness is determined by the local density, covering factor, and shock area as well as by the velocity dispersion.

In radio galaxies, Baum et al. (1992) found abundant evidence for more or less turbulent accretion, and correlations between dynamical factors and observed spectral properties. In

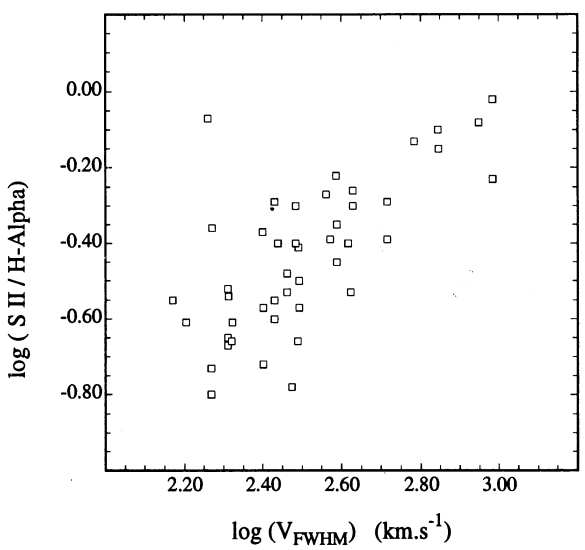

FIG. 8.—An example of a line width–line intensity correlation for luminous IR galaxies with velocity dispersion greater than 250 km s^{-1}. This is taken from the sample of Armus, Heckman, & Miley (1989).

particular, all sources show considerable evidence for turbulent broadening in the range 200–500 km s^{-1}. Those sources characterized by a high ratio of turbulence to rotation show the highest ratios of [N II], [S II], and [O I] to Hα. If these sources are shock-excited, both these properties follow a consequence of the models presented here.

In that paper, they also suggest that the merger events put more angular momentum into the accreting gas, which leads to more rotational support, while nonrotating tubulent flows are associated with cooling flow galaxies. In general, the powerful Fanaroff and Riley class II (FR II) sources are associated with rotationally supported high-ionization nuclear emission (outflow-driven emission on our scenario), while the more amorphous low-power FR I sources are preferentially associated with galaxies which have a nonrotating nebula. In the FR I sources, the gas rotation axis and the radio axis are aligned, suggesting that the latter is determined by the former. This fact, along with the requirement that the emission spectrum of these sources is fitted by the shock + precursor model, suggests that the accretion rates and densities are high in FR II sources but that the FR I sources have LINER-like (shock-only) spectra as a consequence of the lower column densities and physical densities in the nuclear regions.

Finally, although we have argued that many LINERs can be described by shock models, we do not want to exclude the possibility that low-luminosity LINER objects associated with elliptical galaxy cores, such as the sample of nearby elliptical galaxies of Phillips et al. (1986), may be photoionized by post-AGB stars. Strong evidence that the emission in these cases is associated with the stellar, rather than the nuclear, component of these galaxies comes from that fact that, in the sample of Phillips et al., the strength of the emission is strongly correlated with the total galactic luminosity and not with the observed radio luminosity. In fact Caganoff (1989) showed that a clear correlation between radio luminosity and emission luminosity sets in at a critical (radio) luminosity, which corresponds fairly closely to the upper luminosity cutoff of the sample of Phillips et al. This correlation has been much refined by work by Baum, Zirbel, & O'Dea (1995). They find the transition from coreless radio sources having a weak correlation with total radio power to sources having both cores and a strong correlation of total radio power with optical emission to occur at $\sim 10^{25}$ W Hz^{-1} (frequency of 408 MHz). The FR II–FR I transition occurs about an order of magnitude more luminous than this. Binette (1995) has shown that the equivalent width of the emission in low-luminosity LINER galaxies is precisely what is expected on the basis of photoionization by the bare cores of hot post-AGB stars. On the basis of all of this, it therefore seems likely that LINERs are a heterogenous group of objects, which (in order of increasing radio luminosity) make a transition from being photoionized to being shock excited at the Caganoff critical radio luminosity, followed by a further transition from accretion shock–dominated to jet shock–dominated near the FR II–FR I transition.

6. CONCLUSIONS

We believe that this paper has presented strong evidence in favor of a "unified" model for the physics of the narrow-line regions of galaxies; that all these regions are predominantly shock excited by flows of mechanical energy. These may be either associated with jet-powered outflow in the case of Seyfert 2 and 1.5 galaxies, or with accretion in the case of cooling flows and LINERs, or by some combination of these two processes. The major difference separating objects producing LINER-like spectra and those producing Seyfert-like spectra have a sufficient amount of gas beyond the shock to absorb the EUV photons produced in the cooling zone of the shock in an extended preshock H II region, while objects producing LINER-like spectra do not. In this model, ionization cones representing the working surface separating a fast jet from the galactic medium.

We have shown that, apart from shock velocity, the magnetic parameter is a key factor in determining the location of models on the diagnostic diagrams. Increasing shock velocity serves both to increase the ionization parameter in the preshock gas and to harden the emergent EUV radiation field, while an increase in the magnetic parameter serves to increase the ionization parameter in the photoionization-recombination zone of the shock. In this sense these parameters serve the same purpose as the ionization parameter and spectral index in beamed photoionization models of narrow-line regions.

To fit the observed spectra, the shock velocities required to fit LINER spectra range over the full computed range, 150–500 km s^{-1}, but Seyfert spectra require shocks in the range 300–500 km s^{-1}. These are comparable to the observed line widths in both these classes of object. The magnetic parameter which characterizes these shocks is about $2 < B/n^{1/2} < 4$ μG $cm^{3/2}$, typical of the general interstellar medium. Our fast shock models are capable of explaining the long-standing "temperature problem" of AGNs, in which the electron temperatures observed are found to be systematically higher than predicted by photoionization models. For Seyfert galaxies, the preshock densities are clearly higher than the 1 cm^{-3} used in our model grid. We find evidence that nitrogen is enhanced above solar values in both Seyfert and in LINER nuclei.

The shock model has the advantage of providing a natural link between the spectral characteristics, surface brightness, and dynamics of the narrow-line region. Correlations between these quantities are commonly observed but have no simple or natural explanation on the basis of photoionization models. In addition, correlations in the morphology of the narrow-line gas and the nonthermal emission and between narrow-line and nonthermal luminosities can find a sample explanation in terms of a mechanically driven outflow.

A number of parameters and effects remain uninvestigated. First, it is clear that we must investigate the effects of density, finite shock age, limited gas supply through the shock, and chemical abundance on the output spectra. Furthermore, the effect of "fragmentation" discussed by Sutherland et al. (1993) needs to be included. Radiative transfer effects caused by the escape of ionizing photons into low-density regions may also be important in determining the ionization of the gas in the "ionization cones." In the next paper in this series, we will systematically investigate density and abundance effects and also consider the case of "transition" objects in which the precursor H II region is incomplete.

M. A. D. would like to thank Geoff Bicknell, Zlatko Tsvetanov, Holland Ford, Bill Sparks, Andrew Wilson, Ski Antonucci, Wil van Breugel, Gerard Cecil, and Jon Morse for stimulating discussions in the course of this work. We also would like to thank the referee, Sylvain Veilleux, whose constructive comments have contributed greatly to this paper and to whom we are grateful for pointing out to us the importance of shock excitation in LIR galaxies.

REFERENCES

Aldrovandi, S. M. V., & Contini, M. 1984, A&A, 140, 368
———. 1985, A&A, 149, 109
Antonucci, R. R. J., & Miller, J. S. 1985, ApJ, 297, 621
Armus, L., Heckman, T. M., & Miley, G. K. 1989, ApJ, 347, 727
———. 1990, ApJ, 364, 471
Baldwin, J. A., Phillips, M. M., & Terlevich, R. 1981, PASP, 93, 5
Barthel, P. 1989, ApJ, 336, 606
Barvainis, R. 1993, ApJ, 412, 513
Baum, S. A., et al. 1988, ApJS, 68, 643
Baum, S. A., & Heckman, T. M. 1989, ApJ, 336, 702
Baum, S. A., Heckman, T. M., & van Breugel, W. 1992, ApJ, 389, 208
Baum, S. A., Zirbel, E. L., & O'Dea, C. P. 1995, ApJ, 451, 88
Bicknell, G. V. 1990, ApJ, 354, 98
———. 1994, in ASP Conf. Ser. 54, The Physics of Active Galaxies, ed. G. V. Bicknell, M. A. Dopita, & P. J. Quinn (San Francisco: ASP), 231
Binette, L. 1985, A&A, 143, 334
———. 1995, private communication
Binette, L., Dopita, M. A., & Tuohy, I. R. 1985, ApJ, 297, 476
Binette, L., Parker, D., & Fosbury, R. A. E. 1995, preprint
Caganoff, S. 1989, Ph.D. thesis, The Australian National University
Cecil, G. N. 1988, ApJ, 329, 38
Cecil, G. N., & Bland, J. 1989, in IAU Symp. 134, Active Galactic Nuclei, ed. D. E. Osterbrock & J. S. Miller (Dordrecht: Kluwer), 345
Cecil, G. N., Morse, J., & Veilleux, S. 1995, ApJ, 452, 000
Cecil, G. N., Wilson, A. S., & Tully, R. B. 1992, ApJ, 390, 365
Contini, M., & Aldrovandi, S. M. V. 1983, A&A, 127, 15
———. 1986, A&A, 168, 41
Contini, M., & Viegas-Aldrovandi, S. M. 1987, A&A, 185, 39
Costero, R., & Osterbrock, D. E. 1977, ApJ, 211, 675
Cowie, L. L., Hu, E. M., Jenkins, E. B., & York, D. G. 1983, ApJ, 272, 29
Crawford, C. S., & Fabian, A. C. 1992, MNRAS, 259, 265
Daltabuit, E., & Cox, D. 1972, ApJ, 173, L13
De Bruyn, A. G., & Wilson, A. S. 1978, A&A, 64, 433
Diaz, A. I., Pagel, B. E. J., & Terlevich, E. 1985a, MNRAS, 214, 41P
Diaz, A. I., Pagel, B. E. J., & Wilson, I. R. G. 1985b, MNRAS, 212, 737
D'Odorico, S. 1978, Mem. Soc. Astron. Italiana, 49, 485
Dopita, M. A. 1977, ApJS, 33 437
———. 1978, ApJS, 37, 117
Dopita, M. A., Binette, L., D'Odorico, S., & Benvenuti, P. 1984, ApJ, 276, 653
Dopita, M. A., & Meatheringham, S. J. 1990, ApJ, 357, 140
Dopita, M. A., & Sutherland, R. S. 1996, ApJS, in press (Paper I)
Ferland, G. J., & Netzer, H. 1983, ApJ, 264, 105
Forbes, D. A., & Ward, M. J. 1993, ApJ, 416, 150
Fosbury, R. A. E. 1989, in Extranuclear Activity in Galaxies, ed. E. J. A. Meurs & R. A. E. Fosbury (Garching: ESO), 169
Fosbury, R. A. E., Mebold, U., Goss, W. M., & Dopita, M. A. 1978, MNRAS, 183, 549
Heckman, T. M. 1980, A&A, 87, 142
———. 1981, ApJ, 250, L59
Heckman, T. M., Baum, S. A., van Breugel, W. J. M., & McCarthy, P. 1989, ApJ, 338, 48
Ho, L. C., Filippenko, A. V., & Sargent, W. L. 1993, ApJ, 417, 63
Johnstone, R. M., Fabian, A. C., & Nulsen, P. E. J. 1987, MNRAS, 224, 74
Keel, W. C. 1983a, ApJS, 52, 229
———. 1983b, ApJ, 269, 466
Keel, W. C., & Miller, J. G. 1983, ApJ, 266, L89
Khachikian, E. Ye., & Weedman, D. W. 1974, ApJ, 192, 581
Kirhakos, S., & Phillips, M. M. 1989, PASP, 101, 949
Koekemoer, A. M. 1994, in ASP Conf. Ser. 54, The Physics of Active Galaxies, ed. G. V. Bicknell, M. A. Dopita, & P. J. Quinn (San Francisco: ASP), 371
Koski, A. T. 1978, ApJ, 223, 56
Koski, A. T., & Osterbrock, D. E. 1976, ApJ, 203, L89
Kriss, G. A., et al. 1992, ApJ, 394, L37
McCarthy, P. J., van Breugel, W., Spinrad, H., & Djorgovski, S. 1987, ApJ, 321, L29
Meisenheimer, K. Hippelein, H., & Neeser, M. 1994, in ASP Conf. Ser. 54, The Physics of Active Galaxies, ed. G. V. Bicknell, M. A. Dopita, & P. J. Quinn (San Francisco: ASP), 397
Meurer, G. R., Freeman, K. C., & Dopita, M. A. 1989, Ap&SS, 156, 141
Morganti, R., Fosbury, R. A. E., Oosterloo, T. A., & Tadhunter, C. N. 1994, in ASP Conf. Ser. 54, The Physics of Active Galaxies, ed. G. V. Bicknell, M. A. Dopita, & P. J. Quinn (San Francisco: ASP), 267
Morris, S. L., & Ward, M. J. 1988, MNRAS, 230, 639
Mulchaey, J. S., Tsvetanov, Z., Wilson, A. S., & Pérez-Fournon, I. 1992, ApJ, 394, 91
Osterbrock, D. E. 1971, Pontif. Acad. Sci. Scripta Varia, ed. D. J. K. O'Connell, 35, 151
Osterbrock, D. E., Tran, H. D., & Veilleux, S. 1992, ApJ, 389, 196
Pagel, B. E. J., & Edmonds, M. G. 1981, ARA&A, 19, 77
Phillips, M. M., et al. 1986, AJ, 91, 1062
Pogge, R. W. 1988a, ApJ, 328, 519
———. 1988b, ApJ, 332, 702
———. 1989, ApJ, 345, 730
Prieto, A., di Serego Alighieri, S., & Fosbury, R. A. E. 1989, in Extranuclear Activity in Galaxies, ed. E. J. A. Meurs & R. A. E. Fosbury (Garching: ESO), 31
Sabbadin, F., Minello, S., & Bianchini, A. 1977, A&A, 60, 147
Shapiro, P. R., Clocchiatti, A., & Kang, H. 1992, ApJ, 389, 269
Shuder, J. M., & Osterbrock, D. E. 1981, ApJ, 250, 55
Sparks, W. B., Ford, H. C., & Kinney, A. L. 1993, ApJ, 413, 531
Stasinska, G. 1984, A&A, 135, 341
Storchi-Bergmann, T., Kinney, A. L., & Challis, P. 1995, ApJS, 98, 103
Sutherland, R. S., Bicknell, G. V., & Dopita, M. A. 1993, ApJ, 414, 510
Sutherland, R. S., & Dopita, M. A. 1993, ApJS, 88, 253
Tadhunter, C. N., Robinson, A., & Morganti, R. 1989, in Extranuclear Activity in Galaxies, ed. E. J. A. Meurs & R. A. E. Fosbury (Garching: ESO), 293
Tadhunter, C. N., & Tsvetanov, Z., I. 1989, Nature, 341, 422
Tsvetanov, Z. I., Allen, M., & Dopita, M. A. 1995, in preparation
Tsvetanov, Z. I., Fosbury, R. A. E., & Tadhunter, C. N. 1995, ApJ, submitted
Unger, S. W., et al. 1987, MNRAS, 228, 671
van Breugel, W., Miley, G., Heckman, T., Butcher, H., & Bridle, A. 1985, ApJ, 290, 494
Veilleux, S. 1991a, ApJS, 75, 357
———. 1991b, ApJS, 75, 383
Veilleux, S., Cecil, G., Bland-Hawthorn, J., Tully, R. B., Filippenko, A. V., & Sargent, W. L. W. 1994, ApJ, 433, 48
Veilleux, S., Kim, D.-C., Sanders, D. B., Mazzarella, J. M., & Soifer, B. T. 1995, ApJS, 98, 171
Veilleux, S., & Osterbrock, D. E. 1987, ApJS, 63, 295
Veilleux, S., Tully, R. B., & Bland-Hawthorn, J. 1993, AJ, 105, 1318
Viegas-Aldrovandi, S. M., & Contini, M. 1989a, ApJ, 339, 689
———. 1989b, A&A, 215, 253
Whittle, M. 1992, ApJS, 79, 49
———. 1994, ApJS, 91, 491
Wilson, A. S., & Tsvetanov, Z. I. 1994, AJ, 107, 1227
Wilson, A. S., & Willis, A. G. 1980, ApJ, 240, 429